

The two-loop hemisphere soft function

RANDALL KELLEY AND MATTHEW D. SCHWARTZ

*Center for the Fundamental Laws of Nature
Harvard University
Cambridge, MA 02138, USA*

ROBERT M. SCHABINGER

*Instituto de Física Teórica UAM/CSIC
Universidad Autónoma de Madrid
Cantoblanco, E-28049 Madrid, España*

HUA XING ZHU

*Department of Physics and State Key Laboratory of Nuclear Physics and Technology
Peking University
Beijing 100871, China*

Abstract

The hemisphere soft function is calculated to order α_s^2 . This is the first multi-scale soft function calculated to two loops. The renormalization scale dependence of the result agrees exactly with the prediction from effective field theory. This fixes the unknown coefficients of the singular parts of the two-loop thrust and heavy-jet mass distributions. There are four such coefficients, for 2 event shapes and 2 color structures, which are shown to be in excellent agreement with previous numerical extraction. The asymptotic behavior of the soft function has double logs in the $C_F C_A$ color structure, which agree with non-global log calculations, but also has sub-leading single logs for both the $C_F C_A$ and $C_F T_F n_f$ color structures. The general form of the soft function is complicated, does not factorize in a simple way, and disagrees with the Hoang-Kluth ansatz. The exact hemisphere soft function will remove one source of uncertainty on the α_s fits from e^+e^- event shapes.

1 Introduction

There has been significant activity in the last few years in the effective field community to perform accurate calculations of event shapes for e^+e^- colliders. At high energy, the hadronic final states in e^+e^- collisions are dominated by the formation of jets of particles and described by perturbative QCD. Comparison of theoretic calculations of event shapes with the experimentally measured values has led to some of the most precise measurements of the strong coupling constant α_s . The NNLO fixed order calculations in [1, 2, 3, 4] allow the prediction of many events shapes to order α_s^3 . Advances in Soft-Collinear Effective Theory (SCET) [5, 6, 7, 8] have allowed for resummation of large logarithmic corrections to thrust [9, 10, 11] and heavy jet mass [12] to N³LL accuracy and non-perturbative considerations were included for thrust in [13]. These results have been used to extract a value of α_s that is competitive with the world average [14].

Dijet event shapes such as thrust and heavy jet mass demonstrate singular behavior when calculated perturbatively at fixed order due to the appearance of large logarithmic corrections. These large logarithms invalidate a naive expansion in α_s and thus need to be resummed to provide accurate predictions in the dijet limit. In the dijet limit, there is a clear separation between scales. Effective theory techniques rely on a separation between kinematic scales and, through renormalization group (RG) evolution, logarithms of the ratio of these scales can be resummed. Each of the relevant scales is described by different physics, each of which can be calculated using a different theory. The contribution from each can be shown to factorize into a hard contribution, due to physics at the center of mass energy Q , a jet function, due to physics at the jet scale, and a soft function which describes soft gluon emission. The hard and jet functions are known to 2-loops. However, the soft function relevant for thrust or heavy jet mass is only partially known beyond 1-loop [15, 12]. In this paper, the perturbative soft function is computed analytically to order α_s^2 .

Soft functions have been studied for many years, not just in SCET. These soft functions are defined as matrix elements of Wilson lines. For resummation up to the next-to-leading logarithmic order (NLL), all that is needed about the soft function is its anomalous dimension. This can be extracted either from renormalization-group invariance or from the virtual graphs. For example, such calculations have been done for thrust [11], direct photon [16], and dijet production [17, 18, 19, 20]. To go beyond NLL, one needs the finite parts of these soft functions, which are more difficult to calculate because the real emission graphs are needed, and these involve often complicated phase-space cuts. In all cases calculated at 2-loops so far, such as Drell-Yan [22, 23] or $b \rightarrow s\gamma$ [24], the real emission graphs only involve one scale. Multi-scale soft functions, where different constraints are placed on gluons or quarks going in different directions, such as the hemisphere soft function, are likely to play an important role in hadron collisions [21, 25]. At order α_s , the multiple scales are irrelevant, since only one gluon can be emitted. At order α_s^2 or beyond, there can be real emission graphs depending on multiple scales at the same time. It has been suggested [15] that the soft function should depend only on logarithms of these scales, such as $\ln^2(k_L/k_R)$. Whether more complicated scale-independent terms, such as $\text{Li}_2(-k_L/k_R) + \text{Li}_2(-k_R/k_L)$ might appear has been an open question. Understanding the form of these soft functions in more detail will be important for LHC precision jet physics at NNLL and beyond [25].

The hemisphere soft function $S(k_L, k_R, \mu)$ is the probability to have soft radiation with small component k_L going into the left hemisphere and soft radiation with small component k_R going into the right hemisphere. More precisely, in $e^+e^- \rightarrow$ hadron events at center-of-mass energy Q , in the limit that all radiation is much softer than Q , the cross section is given by matrix elements of Wilson lines. These Wilson lines point in the direction of two back-to-back light-like quarks which come from the Born process $e^+e^- \rightarrow \bar{q}q$. Each quark direction defines a hemisphere, which we call left and right and denote with the light-like 4-vectors n^μ and \bar{n}^μ . If the total radiation in the left (right) hemisphere is P_L^μ (P_R^μ), then $S(k_L, k_R, \mu)$ is the matrix element squared to have $k_L = n \cdot P_L$ and $k_R = \bar{n} \cdot P_R$, with all other degrees of freedom integrated over.

The hemisphere soft function is known to have many interesting properties and is conjectured to have others. The factorization theorem for the full hemisphere mass distribution implies that the Laplace transform of the soft function should factorize into the form

$$\tilde{s}(L_1, L_2, \mu) = \tilde{s}_\mu(L_1)\tilde{s}_\mu(L_2)\tilde{s}_f(L_1 - L_2) \quad (1)$$

where $L_1 = \ln x_L \mu$ and $L_2 = \ln x_R \mu$, with x_R and x_L the Laplace conjugate variables to k_L and k_R . The anomalous dimension of the soft function, and the function $\tilde{s}_\mu(L)$, is known exactly to 3-loop order. The function $\tilde{s}_f(L)$ is known exactly only to order α_s . Hoang and Kluth [15] argued that $\tilde{s}_f(L)$ must be a polynomial of at most 2nd order in L , i.e. $\tilde{s}_f(L) = c_2^S + c_{2L}^S L^2$. In this paper, we show that this Hoang-Kluth ansatz does not hold; $\tilde{s}_f(L)$ is much more complicated. Certain moments of $\tilde{s}_f(L)$ contribute to the coefficients of $\delta(\tau)$ and $\delta(\rho)$ in the thrust and heavy-jet mass distributions. These moments were fit numerically in [15] and [12] using numerical calculations of the singular behaviour of these distributions in full QCD with the program EVENT 2. In this paper, we produce these moments analytically and find that they are in excellent agreement with the most accurate available numerical fit [12].

Any L dependence at large L in $\tilde{s}_f(L)$ turns into large logarithmic behavior of the hemisphere mass distribution (*i.e.* $\ln(M_L/M_R)$). Since all of the μ dependence is in $\tilde{s}_\mu(L)$, these large logs are not determined by RG invariance and correspond to so-called “non-global logs”. Dasgupta and Salam calculated the non-global logs for the related left-hemisphere mass distribution in full QCD [26] and found no non-global logs (up to order L^2) for the $C_F n_f T_F$ color structure and an L^2 term with coefficient $-\frac{4\pi^2}{3}$ for the $C_F C_A$ term. We show below that the asymptotic behavior of $\tilde{s}_f(L)$ is indeed of the form $-\frac{4\pi^2}{3} L^2$ for the $C_F C_A$ color structure. We also find that both this color structure and the $C_F n_f T_F$ one have additional non-global single logs. These are especially interesting because the soft function is symmetric in $L \rightarrow -L$, which seems to forbid a linear term. The linear term appears through a complicated analytic function involving polylogarithms which actually asymptotes to $|L|$.

This paper is organized as follows. In section 2 we review the factorization formula for the hemisphere mass distribution and its thrust and heavy-jet mass projections. Section 3 computes the soft function in dimensional regularization. The calculation is complicated, so the results are summarized separately in 3.3. Section 4 discusses the result and presents the renormalized result for the integrated soft function, which can be compared directly to the predictions from SCET. Section 5 gives the previously missing terms in the singular parts of the 2-loop thrust and heavy jet mass distributions, and compares to previous numerical

estimates. Section 6 gives the full integrated hemisphere soft function which is compared to previous conjectures. The asymptotic form of this distribution, which exhibits non-global logs, is discussed in Section 7. Conclusions and implications are discussed in Section 8.

2 Event Shapes and Factorization in SCET

The hemisphere soft function appears in the factorization theorem for the hemisphere mass distribution. The hemispheres are defined with respect to the thrust axis. Thrust itself is defined by

$$T = \max_{\mathbf{n}} \left(\frac{\sum_i |\mathbf{p}_i \cdot \mathbf{n}|}{\sum_i |\mathbf{p}_i|} \right), \quad (2)$$

where the sum is over all momentum 3-vectors \mathbf{p}_i in the event. The thrust axis is the unit 3-vector \mathbf{n} that maximized the expression in parenthesis. We then define the light-like 4-vectors $n^\mu = (1, \mathbf{n})$ and $\bar{n}^\mu = (1, -\mathbf{n})$. In the dijet limit $T \rightarrow 1$ and it is therefore more convenient to define $\tau = 1 - T$ as the thrust variable so that τ is small in the dijet limit.

Once the thrust axis is known, we divide the event into two hemispheres defined by the plane perpendicular to the thrust axis. We define the P_L^μ and P_R^μ to be the 4-vector sum of all of the radiation going into each hemisphere and $M_L = \sqrt{P_L^2}$ and $M_R = \sqrt{P_R^2}$ to be the hemisphere invariant masses. When both M_L and M_R are small compared to the center-of-mass energy, Q , the hemisphere mass distribution factorizes into [9]

$$\frac{1}{\sigma_0} \frac{d^2\sigma}{dM_L^2 dM_R^2} = H(Q^2, \mu) \int dk_L dk_R J(M_L^2 - Qk_L, \mu) J(M_R^2 - Qk_R, \mu) S(k_L, k_R, \mu). \quad (3)$$

Here, σ_0 is the tree level total cross section. $H(Q^2, \mu)$ is the hard function which accounts for the matching between QCD and SCET. $J(p^2)$ is the inclusive jet function which accounts for the matching between an effective field theory with soft and collinear modes to a theory with only soft modes. Finally, the object of interest, $S(k_L, k_R, \mu)$ is the hemisphere soft function, which is derived by integrating out the remaining soft modes.

In the threshold limit (small hemisphere masses), the thrust axis aligns with the jet axis and thrust can be written as the sum of the two hemisphere masses,

$$\tau = \frac{M_L^2 + M_R^2}{Q^2} + \mathcal{O}\left(\frac{M_{L,R}^4}{Q^4}\right) \quad (4)$$

Heavy jet mass ρ is defined to be the larger of the two hemisphere masses, normalized to the center of mass energy Q ,

$$\rho = \frac{1}{Q^2} \max(M_L^2, M_R^2). \quad (5)$$

When ρ is small, both hemisphere masses are small and the event appears as two pencil-like, back to back jets.

The factorization formula can be used to calculate thrust and heavy jet mass in the dijet limit as integrals over the doubly differential hemisphere mass distribution. Explicitly,

$$\frac{d\sigma}{d\tau} = Q^2 \int dM_L^2 dM_R^2 \frac{d^2\sigma}{dM_L^2 dM_R^2} \delta(Q^2\tau - M_L^2 - M_R^2) \quad (6)$$

and

$$\frac{d\sigma}{d\rho} = Q^2 \int dM_L^2 dM_R^2 \frac{d^2\sigma}{dM_L^2 dM_R^2} [\delta(Q^2\rho - M_L^2)\theta(M_L^2 - M_R^2) + \delta(Q^2\rho - M_R^2)\theta(M_R^2 - M_L^2)] . \quad (7)$$

The thrust distribution can be written so that it depends not on the full hemisphere soft function but on the thrust-soft function, defined as

$$S_T(k, \mu) = \int dk_L dk_R S(k_L, k_R, \mu) \delta(k - k_L - k_R) . \quad (8)$$

Since the thrust soft function is dimensionless and its μ dependence is determined by renormalization group invariance, the k dependence is also completely known. Thus at each order in α_s only one number, the constant part, is unknown. In contrast, for the heavy jet mass distribution, the full k_L and k_R dependence of the soft function is needed for the factorization theorem. In particular, for resummation to N³LL order, only one number is needed for thrust (the constant in the 2-loop thrust soft function), which has been fit numerically, but for heavy-jet mass a function is needed [12]. In this paper we compute both the number and the function.

3 Calculation of the Soft Function

The soft function is defined as

$$S(k_L, k_R, \mu) \equiv \frac{1}{N_c} \sum_{X_s} \delta(k_R - n \cdot P_s^R) \delta(k_L - \bar{n} \cdot P_s^L) \langle 0 | \bar{Y}_{\bar{n}} Y_n | X_s \rangle \langle X_s | Y_n^\dagger \bar{Y}_{\bar{n}}^\dagger | 0 \rangle , \quad (9)$$

where $P_s^{L,R}$ is the total momentum of the final state $|X_s\rangle$ in the left and right hemisphere, respectively. The Wilson lines Y_n and $\bar{Y}_{\bar{n}}$ are defined by

$$Y_n^\dagger(x) = P \exp \left(ig \int_0^\infty ds n \cdot A_s(ns + x) \right) \quad \bar{Y}_{\bar{n}}^\dagger(x) = P \exp \left(ig \int_0^\infty ds \bar{n} \cdot \bar{A}_s(ns + x) \right) , \quad (10)$$

where P denotes path ordering and $A_s = A_s^a T^a$ ($\bar{A}_s = A_s^a \bar{T}^a$) are gauge fields in the fundamental (anti-fundamental) representation. The soft function can be factorized into a perturbative (partonic) part and non-perturbative part which has support of order Λ_{QCD} [13].

The authors of [15] observed that the form of the soft function is constrained by the non-Abelian exponentiation theorem and RG invariance, which puts constraints on powers of logarithms of μ . The theorem also restricts the C_F^n color structure in the soft function to be completely determined by the one-loop result. Beyond this, however, the soft function is unconstrained. The one-loop calculation was done in [9, 27]. The main result of this paper is the calculation of the perturbative part of the hemisphere soft function to order α_s^2 . Since the order α_s^2 color structure C_F^2 is given in [15], we will only calculate the $C_F C_A$ and the $C_F n_f T_F$ terms.

3.1 $C_F C_A$ color structure

The order α_s^2 calculation involves pure virtual graphs, pure real emission graphs, and interference between the two. The pure virtual contributions to the soft function give scaleless integrals which convert IR divergences to UV divergences, and are not explicitly written. The diagrams needed to compute the pure real emission contributions are shown in Figs. 1-4, whereas the interference graphs between the order α_s real and virtual emission amplitudes are shown in Fig. 5.

The integrals corresponding to the two diagrams in Fig. 1 (and the twin of diagram A obtained by interchanging k and q) are given, in $d = 4 - 2\epsilon$ dimensions using the $\overline{\text{MS}}$ scheme, by

$$I_A = 2(-4g^4) \left(C_F^2 - \frac{C_F C_A}{2} \right) \left(\frac{\mu^2 e^{\gamma_E}}{4\pi} \right)^{2\epsilon} \int \frac{d^d q}{(2\pi)^d} \int \frac{d^d k}{(2\pi)^d} \frac{1}{k^- k^+ q^- q^+} F(k_L, k_R) \quad (11)$$

and

$$I_B = -4g^4 \left(\frac{\mu^2 e^{\gamma_E}}{4\pi} \right)^{2\epsilon} \int \frac{d^d q}{(2\pi)^d} \int \frac{d^d k}{(2\pi)^d} \frac{1}{(k^+ + q^+)(k^- + q^-)} \\ \times \left\{ \left(C_F^2 - \frac{C_F C_A}{2} \right) \left(\frac{1}{k^- k^+} + \frac{1}{q^- q^+} \right) + C_F^2 \left(\frac{1}{k^- q^+} + \frac{1}{q^- k^+} \right) \right\} F(k_L, k_R), \quad (12)$$

where $k^- = \bar{n} \cdot k$, $k^+ = n \cdot k$ and $F(k_L, k_R)$ contains the $\delta(q^2)$ and $\delta(k^2)$ factors which put the emitted gluons on shell and the phase-space restrictions in the definition of the hemisphere soft function. Explicitly, $F(k_L, k_R)$ is given by

$$F(k_L, k_R) = \frac{1}{2!} (-2\pi i)^2 \delta(k^2) \delta(q^2) \\ \times \left[\Theta(k^- - k^+) \Theta(q^+ - q^-) \delta(k^+ - k_R) \delta(q^- - k_L) \right. \\ + \Theta(k^+ - k^-) \Theta(q^- - q^+) \delta(k^- - k_L) \delta(q^+ - k_R) \\ + \Theta(k^- - k^+) \Theta(q^- - q^+) \delta(k^+ + q^+ - k_R) \delta(k_L) \\ \left. + \Theta(q^+ - q^-) \Theta(k^+ - k^-) \delta(k^- + q^- - k_L) \delta(k_R) \right]. \quad (13)$$

In each diagram, the momentum has been routed so that the 4-vectors k and q correspond to the final state gluons. The gluonic contribution to the $C_F C_A$ color factor will be symmetric in k and q due to the fact that the radiated gluons are identical particles. In the first diagram, a factor of two has been added since the integrand is unchanged after $k \leftrightarrow q$, whereas in the second diagram, the SCET Feynman rules for two gluon emission from a single soft Wilson line automatically account for $k \leftrightarrow q$. The factor of $1/2!$ needed for averaging over $k \leftrightarrow q$ is in $F(k_L, k_R)$. Not shown in Fig. 1 is the graph that corresponds to the complex conjugate of diagram B. This diagram gives the same integral as diagram B. Since we are interested in the $C_F C_A$ contribution, the linear combination of interest is $I_A + 2I_B$. Diagram A and its

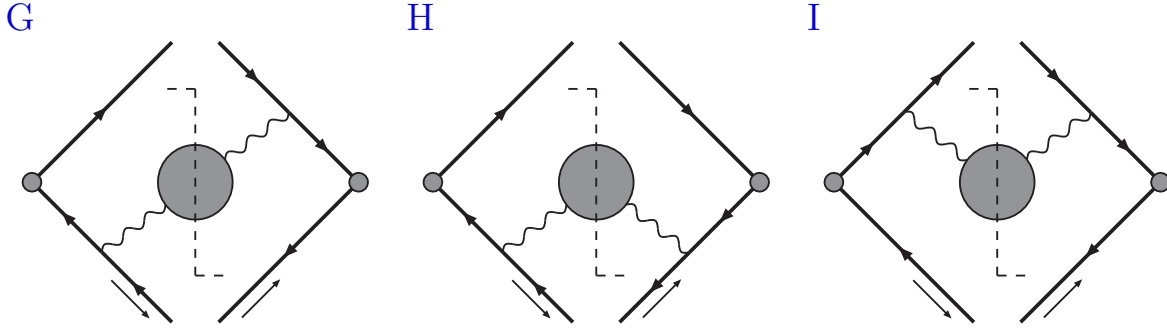


Figure 4: Diagrams **G**, **H** and **I**. These classes of diagrams contribute to integrals I_G, I_H , and I_I when the self-energy graphs involve gluons or ghosts and they contribute to integrals \tilde{I}_G, \tilde{I}_H , and \tilde{I}_I when the self-energy graphs involve a fermion/anti-fermion pair.

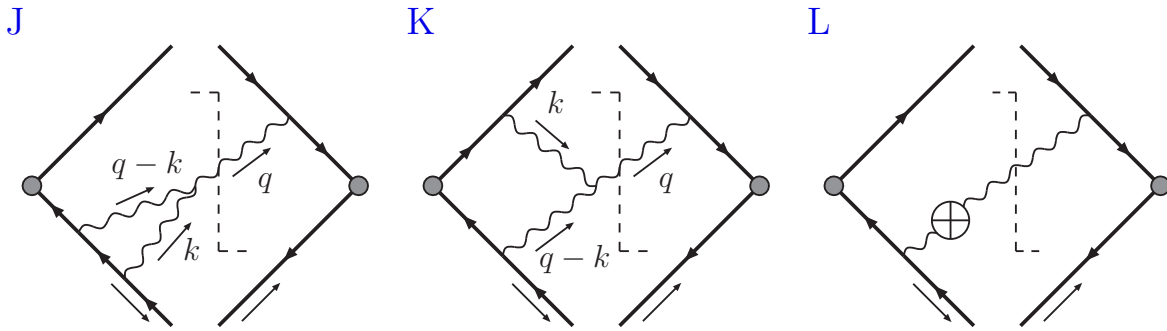


Figure 5: Diagrams **J** and **K** account for the interference between the one-loop virtual emission amplitude and the single gluon emission amplitude. Diagram **L** is the contribution from charge renormalization.

identical twin are self-conjugate and only contribute once because they represent the squares of tree-level Feynman diagrams.

There are four classes of diagrams involving the triple gauge coupling. Diagrams **C** and **D**, shown in Fig. 2, give the following integrals,

$$I_C = -g^4 C_A C_F \left(\frac{\mu^2 e^{\gamma_E}}{4\pi} \right)^{2\epsilon} \int \frac{d^d q}{(2\pi)^d} \int \frac{d^d k}{(2\pi)^d} \frac{F(k_L, k_R)}{(k^- + q^-)(k + q)^2} \left(\frac{k^- + 2q^-}{k^+ q^-} + \frac{q^- + 2k^-}{q^+ k^-} \right) \quad (14)$$

$$I_D = -g^4 C_A C_F \left(\frac{\mu^2 e^{\gamma_E}}{4\pi} \right)^{2\epsilon} \int \frac{d^d q}{(2\pi)^d} \int \frac{d^d k}{(2\pi)^d} \frac{F(k_L, k_R)}{(k^+ + q^+)(k + q)^2} \left(\frac{2k^+ + q^+}{k^+ q^-} + \frac{2q^+ + k^+}{q^+ k^-} \right) \quad (15)$$

whereas, diagrams **E** and **F**, shown in Fig 3, give

$$I_E = g^4 C_F C_A \left(\frac{\mu^2 e^{\gamma_E}}{4\pi} \right)^{2\epsilon} \int \frac{d^d q}{(2\pi)^d} \int \frac{d^d k}{(2\pi)^d} \times \left(\frac{1}{q^-} - \frac{1}{k^-} \right) \frac{q^- - k^-}{(k^+ + q^+)(k^- + q^-)(k + q)^2} F(k_L, k_R)$$

$$I_F = g^4 C_F C_A \left(\frac{\mu^2 e^{\gamma_E}}{4\pi} \right)^{2\epsilon} \int \frac{d^d q}{(2\pi)^d} \int \frac{d^d k}{(2\pi)^d} \times \left(\frac{1}{k^+} - \frac{1}{q^+} \right) \frac{k^+ - q^+}{(k^+ + q^+)(k^- + q^-)(k + q)^2} F(k_L, k_R)$$

Each of these diagrams has a complex conjugate and so they contribute twice.

There are three self-energy topologies, shown in Fig. 4. The gluon and ghost self-energy graphs contribute to integrals I_G , I_H and I_I below.

$$I_G = g^4 C_F C_A \left(\frac{\mu^2 e^{\gamma_E}}{4\pi} \right)^{2\epsilon} \int \frac{d^d q}{(2\pi)^d} \int \frac{d^d k}{(2\pi)^d} \frac{1}{(k^- + q^-)(k^+ + q^+)(k + q)^4} \times \left[q^+ [(d-6)q^- - (d+2)k^-] + k^+ [(d-6)k^- - (d+2)q^-] + 16k \cdot q \right] F(k_L, k_R)$$

$$I_H = g^4 C_F C_A \left(\frac{\mu^2 e^{\gamma_E}}{4\pi} \right)^{2\epsilon} \int \frac{d^d q}{(2\pi)^d} \int \frac{d^d k}{(2\pi)^d} \frac{1}{(k^- + q^-)^2 (k + q)^4} \times \left[2(d+2)q^- k^- - (d-6)(k^-)^2 - (d-6)(q^-)^2 \right] F(k_L, k_R)$$

$$I_I = g^4 C_F C_A \left(\frac{\mu^2 e^{\gamma_E}}{4\pi} \right)^{2\epsilon} \int \frac{d^d q}{(2\pi)^d} \int \frac{d^d k}{(2\pi)^d} \frac{1}{(k^+ + q^+)^2 (k + q)^4} \\ \times \left[2(d+2)q^+ k^+ - (d-6)(k^+)^2 - (d-6)(q^+)^2 \right] F(k_L, k_R)$$

As usual, cutting Feynman diagrams removes any symmetry factors that were associated to the cut lines prior to cutting. It is also worth reminding the reader that, in order to consistently combine the ghost emission diagrams with the gluon emission diagrams, we have to double-count the ghosts (they do not have the $1/2!$ symmetry factor that the gluons do). Diagram **G** has a complex conjugate graph which must be included but diagrams **H** and **I**, like diagram **A**, represent squares of tree-level Feynman diagrams and are therefore self-conjugate.

Adding all of these contributions together, we have

$$S_{C_A}^R(k_L, k_R) = I_A + I_H + I_I + 2(I_B + I_C + I_D + I_E + I_F + I_G) \quad (C_F C_A \text{ part}) \\ = g^4 C_F C_A \left(\frac{\mu^2 e^{\gamma_E}}{4\pi} \right)^{2\epsilon} \int \frac{d^d q}{(2\pi)^d} \int \frac{d^d k}{(2\pi)^d} \left\{ \frac{2}{(k \cdot q)^2 k^- k^+ q^- q^+ (k^- + q^-)(k^+ + q^+)} \right. \\ \times \left[-k \cdot q \left((k^-)^2 q^+ (2k^+ + q^+) + 2k^- q^- \left((k^+)^2 - k^+ q^+ + (q^+)^2 \right) + k^+ (q^-)^2 (k^+ + 2q^+) \right) \right. \\ \left. \left. + 2(k \cdot q)^2 \left(k^- (2k^+ + q^+) + q^- (k^+ + 2q^+) \right) \right] \right. \\ \left. + (\epsilon - 1) \frac{2(k^+ q^- - k^- q^+)^2}{(k \cdot q)^2 (k^- + q^-)^2 (k^+ + q^+)^2} \right\} F(k_L, k_R). \quad (16)$$

Before presenting the result for the $C_F C_A$ color factor, we briefly describe our general computational strategy. Normally, one expects scaleless integrals to be simpler than single scale integrals. In this particular case, the single scale integrals (with scale k_L/k_R) are actually much less technically demanding. This is true primarily because these contributions (see the first two terms of Eq. (13)) are integrable at $\epsilon = 0$. It turns out that this special feature of the problem more than makes up for the fact that single scale integrals are generically harder to evaluate than scaleless integrals.

The calculation proceeds as follows for a single scale integral. First there will be an integral over angles (the integrand depends non-trivially on $k \cdot q$) that can be done analytically to all orders in ϵ . It is then convenient to Taylor series expand the resulting hypergeometric functions using the HypExp package [28] for MATHEMATICA. In fact, the whole integrand can be expanded in a Taylor series in ϵ and integrated term-by-term, due to the fact that the integral converges at $\epsilon = 0$. With a modest amount of knowledge of the basic functional identities satisfied by the polylogarithm functions, it is possible to do the resulting two-fold one-parameter integral in MATHEMATICA and express the final result in terms of a minimal basis of transcendental functions. The results of our single scale calculations for both non-trivial color factors are tabulated in the Appendix.

The evaluation of a scaleless integral (originating from the last two terms of Eq. (13)) begins in much the same way. Unfortunately, it quickly becomes clear that what remains after integrating over all angles has a non-trivial analytical structure (considered as a function of

ϵ). In particular, the integral diverges at $\epsilon = 0$. Expanding an integral of this class under the integral sign is significantly more complicated and requires new tools. To begin, one should transform all hypergeometric functions in the integrand and expose their singularity structure. In this fashion, one learns that there is a line of singularities within the region of integration. A well-known procedure called sector decomposition [29] allows one to move singularities within the region of integration to singularities on the boundaries of the region of integration. Sector decomposition works as follows. Through a sequence of variable changes and interchanges of integration orders, all phase-space singularities are put into a canonical form. At this point, one can use an expansion in distributions to extract singularities in ϵ under the integral sign. Finally, the entire integrand can be expanded in ϵ in terms of distributions and ordinary functions and one can integrate the Laurent series term-by-term.

Once we understood the computational procedure described above, it was straightforward to evaluate the integrals of interest for the $C_F C_A$ color factor. The result has the form

$$S_{C_A}^R(k_L, k_R) = \left(\frac{\alpha}{4\pi}\right)^2 C_F C_A \left[\frac{\mu^{4\epsilon}}{(k_R k_L)^{1+2\epsilon}} f_{C_A} \left(\frac{k_L}{k_R}, \epsilon \right) + \left(\frac{\mu^{4\epsilon}}{k_L^{1+4\epsilon}} \delta(k_R) + \frac{\mu^{4\epsilon}}{k_R^{1+4\epsilon}} \delta(k_L) \right) g_{C_A}(\epsilon) \right].$$

The first term corresponds to the first two terms in Eq. (13), those that account for the possibility that exactly one gluon is radiated into each hemisphere. It depends on $f_{C_A}(r, \epsilon)$, a dimensionless function of $r = k_L/k_R$ and ϵ . It can be written as an expansion in ϵ as

$$f_{C_A}(r, \epsilon) = f_{C_A}^{(0)}(r) + \epsilon f_{C_A}^{(1)}(r) + \epsilon^2 f_{C_A}^{(2)}(r) + \dots. \quad (17)$$

The expressions for $f_{C_A}^{(n)}(r)$ are quite lengthy and are given in the appendix for $n = 0, 1, 2$. The second term in Eq. (17) accounts for the fact that both gluons can propagate into the same hemisphere and it has no non-trivial k_L or k_R dependence. $g_{C_A}(\epsilon)$ is simply a constant with ϵ expansion

$$g_{C_A}(\epsilon) = \frac{4}{\epsilon^3} + \frac{22}{3\epsilon^2} + \frac{1}{\epsilon} \left(\frac{134}{9} - \frac{4\pi^2}{3} \right) - \frac{116\zeta_3}{3} + \frac{11\pi^2}{9} + \frac{772}{27} + \left(\frac{484\zeta_3}{9} + \frac{4784}{81} + \frac{67\pi^2}{27} - \frac{137\pi^4}{90} \right) \epsilon. \quad (18)$$

The interference between the one-loop and tree-level single gluon emission amplitudes is shown in diagrams **J** and **K** of Fig. 5. The integrals associated with diagram **J** are scaleless and are set to zero in dimensional regularization. Diagram **K** gives the integral

$$I_K = 4(-g^4) C_A C_F \int \frac{d^d q}{(2\pi)^d} \frac{1}{q^-} \int \frac{d^d k}{(2\pi)^d} \frac{2q^- - k^-}{k^+ (q^- - k^-) (q - k)^2 k^2} \times (-2\pi i) \delta(q^2) [\Theta(q^- - q^+) \delta(q^+ - k_R) \delta(k_L) + \Theta(q^+ - q^-) \delta(q^- - k_L) \delta(k_R)]. \quad (19)$$

There are 2 diagrams with the topology of diagram **K**. When they are considered with single real emission phase-space cuts, they can easily be mapped into each other and therefore give identical results. Both diagrams also have a complex conjugate graph and these obviously

give equal contributions as well. This is why I_K has an overall factor of 4 out front. After evaluating this integral, the real-virtual interference contribution becomes

$$S_{C_A}^V(k_L, k_R) = \left(\frac{\alpha}{4\pi}\right)^2 C_F C_A \left(\frac{\mu^{4\epsilon}}{k_L^{1+4\epsilon}} \delta(k_R) + \frac{\mu^{4\epsilon}}{k_R^{1+4\epsilon}} \delta(k_L) \right) v_{C_A}(\epsilon), \quad (20)$$

where $v_{C_A}(\epsilon)$ can be expanded in ϵ as

$$v_{C_A}(\epsilon) = -\frac{4}{\epsilon^3} + \frac{2\pi^2}{\epsilon} + \frac{32\zeta_3}{3} - \epsilon \frac{\pi^4}{30}. \quad (21)$$

It is worth noting that, in this case, the application of the optical theorem for Feynman diagrams is a bit subtle; one finds an explicit factor of $\exp(\pm i\pi\epsilon)$ after doing the k integral (the sign of the phase depends on the precise pole prescription). Cutkosky's rules still apply provided that one keeps only the appropriate projection of the complex phase. After a moment's thought it becomes clear that the real part, $\cos(\pi\epsilon)$ (*independent* of the pole prescription), is what one needs to keep to complete the calculation and derive the above result.

The result of diagram L, including the complex conjugate graph, is given by

$$S^{\text{Ren}}(k_L, k_R) = -\left(\frac{\alpha}{4\pi}\right)^2 C_F \left(\frac{\mu^{2\epsilon}}{k_L^{1+2\epsilon}} \delta(k_R) + \frac{\mu^{2\epsilon}}{k_R^{1+2\epsilon}} \delta(k_L) \right) \frac{4e^{\gamma_E}}{\epsilon^2 \Gamma(1-\epsilon)} \beta_0 \quad (22)$$

where $\beta_0 = \frac{11}{3}C_A - \frac{4}{3}n_f T_F$ is the first expansion coefficient of the QCD β -function, $\beta(g)/g = \frac{\alpha_s}{4\pi} \beta_0$. Finally, the total contribution to the $C_F C_A$ color factor is given by

$$S_{C_A}(k_L, k_R) = S_{C_A}^R(k_L, k_R) + S_{C_A}^V(k_L, k_R) + S_{C_A}^{\text{Ren}}(k_L, k_R), \quad (23)$$

where $S_{C_A}^{\text{Ren}}$ is the $C_F C_A$ part of S^{Ren} .

3.2 $C_F n_f T_F$ color structure

The diagrams involving a fermion loop contribute to the $C_F n_f T_F$ color factor and give integrals \tilde{I}_G , \tilde{I}_H , and \tilde{I}_I . The first topology in Fig. 4, where the blob now represents a fermion loop, gives

$$\tilde{I}_G = g^4 C_F n_f T_F \left(\frac{\mu^2 e^{\gamma_E}}{4\pi} \right)^{2\epsilon} \int \frac{d^d q}{(2\pi)^d} \int \frac{d^d k}{(2\pi)^d} \frac{4(k^+ q^- + k^- q^+ - 2k \cdot q)}{(k^+ + q^+)(k^- + q^-)(k + q)^4} F_{n_f}(k_L, k_R). \quad (24)$$

The phase-space cut is accounted for by

$$\begin{aligned} F_{n_f}(k_L, k_R) &= (-2\pi i)^2 \delta(k^2) \delta(q^2) \\ &\times \left[\Theta(k^- - k^+) \Theta(q^+ - q^-) \delta(k^+ - k_R) \delta(q^- - k_L) + \Theta(k^+ - k^-) \Theta(q^- - q^+) \delta(k^- - k_L) \delta(q^+ - k_R) \right. \\ &\left. + \Theta(k^- - k^+) \Theta(q^- - q^+) \delta(k^+ + q^+ - k_R) \delta(k_L) + \Theta(q^+ - q^-) \Theta(k^+ - k^-) \delta(k^- + q^- - k_L) \delta(k_R) \right]. \end{aligned}$$

The complex conjugate of this diagram gives the same result, so \tilde{I}_g contributes twice. For the second and third topologies shown in Fig. 4, we get

$$\tilde{I}_H = g^4 C_F n_f T_F \left(\frac{\mu^2 e^{\gamma_E}}{4\pi} \right)^{2\epsilon} \int \frac{d^d q}{(2\pi)^d} \int \frac{d^d k}{(2\pi)^d} \frac{-8k^+ q^+}{(k^+ + q^+)^2 (k + q)^4} F_{n_f}(k_L, k_R) \quad (25)$$

and

$$\tilde{I}_I = g^4 C_F n_f T_F \left(\frac{\mu^2 e^{\gamma_E}}{4\pi} \right)^{2\epsilon} \int \frac{d^d q}{(2\pi)^d} \int \frac{d^d k}{(2\pi)^d} \frac{-8k^- q^-}{(k^- + q^-)^2 (k + q)^4} F_{n_f}(k_L, k_R). \quad (26)$$

The sum of these contributions is

$$\begin{aligned} S_{n_f}^R(k_L, k_R) &= 2\tilde{I}_G + \tilde{I}_H + \tilde{I}_I \\ &= g^4 C_F n_f T_F \left(\frac{\mu^2 e^{\gamma_E}}{4\pi} \right)^{2\epsilon} \int \frac{d^d q}{(2\pi)^d} \int \frac{d^d k}{(2\pi)^d} \\ &\quad \times \frac{8}{(k + q)^4} \left(\frac{k^+ q^- + k^- q^+ - 2k \cdot q}{(k^+ + q^+)(k^- + q^-)} - \frac{k^- q^-}{(k^- + q^-)^2} - \frac{k^+ q^+}{(k^+ + q^+)^2} \right) F_{n_f}(k_L, k_R) \end{aligned} \quad (27)$$

Evaluating this integral gives

$$S_{n_f}^R(k_L, k_R) = \left(\frac{\alpha}{4\pi} \right)^2 C_F n_f T_F \left[\frac{\mu^{4\epsilon}}{(k_R k_L)^{1+2\epsilon}} f_{n_f} \left(\frac{k_L}{k_R}, \epsilon \right) + \left(\frac{\mu^{4\epsilon}}{k_L^{1+4\epsilon}} \delta(k_R) + \frac{\mu^{4\epsilon}}{k_R^{1+4\epsilon}} \delta(k_L) \right) g_{n_f}(\epsilon) \right].$$

As in the $C_F C_A$ case, the first term corresponds to the quark and anti-quark propagating into different hemispheres and it depends on $r = k_L/k_R$ in a non-trivial way through a function $f_{n_f}(r, \epsilon)$. $f_{n_f}(r, \epsilon)$ can be expanded in a Taylor series in ϵ as

$$f_{n_f}(r, \epsilon) = f_{n_f}^{(0)}(r) + \epsilon f_{n_f}^{(1)}(r) + \dots \quad (28)$$

The expressions for $f_{n_f}^{(n)}(r)$ are given in the appendix for $n = 0, 1$. For the $C_F n_f T_F$ color factor $n = 2$ plays no role due to the fact that $f_{n_f}^{(n)}(0) = f_{n_f}^{(n)}(\infty) = 0$.

The second term Eq. (28) is present because both the quark and anti-quark may propagate into the same hemisphere as well. As before, this contribution has no non-trivial k_L or k_R dependence. The constant g_{n_f} has a series expansion

$$g_{n_f}(\epsilon) = -\frac{8}{3\epsilon^2} - \frac{40}{9\epsilon} - \frac{152}{27} - \frac{4\pi^2}{9} + \left(-\frac{952}{81} - \frac{20\pi^2}{27} - \frac{176\zeta_3}{9} \right) \epsilon. \quad (29)$$

The final contribution to this color factor is from the charge renormalization, diagram **L**, the results of which were given in Eq. (22). Adding this contribution to the real emission contributions yields the final result for the $C_F n_f T_F$ color factor. It is

$$S_{n_f}(k_L, k_R) = S_{n_f}^R(k_L, k_R) + S_{n_f}^{\text{Ren}}(k_L, k_R), \quad (30)$$

where $S_{n_f}^{\text{Ren}}$ is the $C_F n_f T_F$ part of S^{Ren} .

3.3 Summary of the Calculation

In summary, we found that the 2-loop hemisphere soft function in $d = 4 - 2\epsilon$ dimensions has the form

$$S(k_L, k_R, \mu) = \left(\frac{\alpha}{4\pi}\right)^2 \left[\frac{\mu^{4\epsilon}}{(k_R k_L)^{1+2\epsilon}} f\left(\frac{k_L}{k_R}, \epsilon\right) + \left(\frac{\mu^{4\epsilon}}{k_L^{1+4\epsilon}} \delta(k_R) + \frac{\mu^{4\epsilon}}{k_R^{1+4\epsilon}} \delta(k_L) \right) h(\epsilon) - 4C_F \beta_0 \left(\frac{\mu^{2\epsilon}}{k_L^{1+2\epsilon}} \delta(k_R) + \frac{\mu^{2\epsilon}}{k_R^{1+2\epsilon}} \delta(k_L) \right) \frac{e^{\gamma_E}}{\epsilon^2 \Gamma(1-\epsilon)} \right]. \quad (31)$$

Here $f(r, \epsilon) = f(1/r, \epsilon)$ is the opposite-direction contribution (where the two gluons or two quarks go into opposite hemispheres) and $h(\epsilon)$ is the same-direction contribution. Since all the μ dependence is shown explicitly, $h(\epsilon)$ cannot depend on k_L or k_R by dimensional analysis. The second line is the contribution that comes from the interference of the first non-trivial term in the expansion of the charge renormalization constant and the $\mathcal{O}(\alpha_s)$ hemisphere soft function. It is proportional to $\beta_0 = \frac{11}{3}C_A - \frac{4}{3}T_F n_f$.

There are 3 color structures, C_F^2 , $C_F C_A$ and $C_F n_f T_F$. The C_F^2 color structure is trivial – by non-Abelian exponentiation it is the square of the one-loop result. For the other two color structures the function $f(r, \epsilon)$ is complicated. In both cases it is finite at $\epsilon = 0$, and in the $C_F n_f T_F$ case, $f_{n_f}(0, \epsilon) = f_{n_f}(\infty, \epsilon) = 0$. We write

$$f(r, \epsilon) = f^{(0)}(r) + \epsilon f^{(1)}(r) + \epsilon^2 f^{(2)}(r) \quad (32)$$

The expansions in ϵ of $f(r, \epsilon)$ for the two color structures are given in the Appendix. Due to the fact that $f_{n_f}(0, \epsilon) = f_{n_f}(\infty, \epsilon) = 0$, $f_{n_f}^{(2)}(r)$ does not contribute to the renormalized soft function and is not given.

For the same direction contribution, $h(\epsilon)$, there are contributions from the real-emission diagrams and, for the $C_F C_A$ color structure, interference between tree-level real emission and one-loop real-virtual graphs. The real emission contributions we called $g(\epsilon)$, and are given in Eqs. (18) and (29). The interference graphs are given by $v_{C_A}(\epsilon)$ in Eq. (21). Adding these terms we get for the $C_F C_A$ color structure

$$h_{C_A}(\epsilon) = \frac{22}{3\epsilon^2} + \frac{134}{9} + \frac{2\pi^2}{3} - 28\zeta_3 + \frac{11\pi^2}{9} + \frac{772}{27} + \left(\frac{484\zeta_3}{9} + \frac{4784}{81} + \frac{67\pi^2}{27} - \frac{14\pi^4}{9} \right) \epsilon \quad (33)$$

and for completeness, copying Eq. (29)

$$h_{n_f}(\epsilon) = -\frac{8}{3\epsilon^2} - \frac{40}{9\epsilon} - \frac{152}{27} - \frac{4\pi^2}{9} + \left(-\frac{952}{81} - \frac{20\pi^2}{27} - \frac{176\zeta_3}{9} \right) \epsilon. \quad (34)$$

4 Integrating the soft function

Now we would like to expand and renormalize the soft function. At one-loop, all that is necessary for the expansion is the relation

$$\frac{\mu^{4\epsilon}}{k^{1+2\epsilon}} = -\frac{1}{2\epsilon} \delta(k) + \left[\frac{1}{k} \right]_* - 2\epsilon \left[\frac{\ln \frac{k}{\mu}}{k} \right]_* + \dots, \quad (35)$$

where the $*$ -distributions are defined, for example, in [9]. Unfortunately, this expansion cannot be used separately for k_L and k_R , since the region where they both go to zero is not well-defined. For example, what does $\delta(k_L)\delta(k_R)f(k_L/k_R)$ mean? If we take $k_L \rightarrow 0$ first, then $k_R \rightarrow 0$, then we pick up $f(0)$. If we take $k_L, k_R \rightarrow 0$ holding $k_L = k_R$, then we pick up $f(1)$. Unless $f(r)$ is constant, one must do the expansion more carefully.

A simple solution is just to expand in distributions of $p = k_L k_R$ and $r = k_L/k_R$. This expansion is well-defined, and can be used to integrate any observable, such as thrust or heavy jet mass against the hemisphere soft function. For example, consider the integrated soft function:

$$\mathcal{R}(X, Y, \mu) \equiv \int_0^X dk_L \int_0^Y dk_R s(k_L, k_R, \mu). \quad (36)$$

This function contains the entire soft contribution to the integrated doubly differential hemisphere mass distribution. Since it is a function, rather than a distribution, we can use this integrated form to check the μ -dependence and compare to previous predictions.

We can calculate $\mathcal{R}(X, Y, \mu)$ using Eq. (31) and the expansion in Eq. (35). For the same direction contribution (the real emission graphs, real/virtual interference graphs, and charge renormalization), the soft function is trivial to integrate in d dimensions. For the opposite direction contribution, the integral of the distributions is complicated by the overlapping singularities. It is a straightforward exercise in sector decomposition [29] to isolate the singularities and perform the integrations. The result can then be renormalized in $\overline{\text{MS}}$. We find, for the opposite direction contribution,

$$\begin{aligned} \mathcal{R}(X, Y, \mu) = \left(\frac{\alpha_s}{4\pi}\right)^2 & \left\{ \frac{1}{4} f^{(2)}(0) - \frac{1}{2} f^{(1)}(0) \ln \frac{XY}{\mu^2} + \frac{1}{2} f^{(0)}(0) \ln^2 \frac{XY}{\mu^2} \right. \\ & - \frac{1}{2} \int_0^1 dz \left[\frac{1}{z} \right]_+ f^{(1)}(z) + \int_0^1 dz \left[\frac{\ln z}{z} \right]_+ f^{(0)}(z) + \ln \frac{XY}{\mu^2} \int_0^1 dz \left[\frac{1}{z} \right]_+ f^{(0)}(z) \\ & \left. - \frac{1}{2} \int_1^{Y/X} dy \int_1^{Y/X} dx \frac{f^{(0)}(x/y) - f^{(0)}(0)}{xy} \right\}, \quad (37) \end{aligned}$$

where $f^{(n)}(r)$ refer to the coefficients in the expansion in Eq. (32). The final compiled results for $\mathcal{R}(X, Y, \mu)$ for the different color structures, including the same-direction and opposite direction contributions, are given in Sec. 6.

The integrated soft function directly gives us the α_s^2 soft function contribution to the integrated order α_s^2 heavy jet mass distribution,

$$R_\rho(\rho) = \frac{1}{\sigma_0} \int_0^\rho \frac{d\sigma}{d\rho'} d\rho' = \mathcal{R}(\rho Q, \rho Q, \mu). \quad (38)$$

For thrust, the integrated distribution is not given in trivial way from the integrated soft function. However, it differs from the heavy-jet mass distribution only by a single finite integral

$$R_\tau(\tau) = \frac{1}{\sigma_0} \int_0^\tau \frac{d\sigma}{d\tau'} d\tau' = R_\rho(\tau) - \left(\frac{\alpha_s}{4\pi}\right)^2 \int_0^1 dx \int_{1-x}^1 dy \frac{f^{(0)}(x/y)}{xy} \quad (39)$$

which we can now compute for the $C_F C_A$ and $C_F n_f T_F$ color structures. Adding also the C_F^2 terms, which were already known, the result is

$$R_\tau(\tau) = R_\rho(\tau) + \left(\frac{\alpha_s^2}{4\pi}\right)^2 \left[-\frac{8\pi^4}{45} C_F^2 + \left(\frac{8}{3} - 8\zeta_3\right) C_F n_f T_F \right. \\ \left. + \left(32\text{Li}_4\frac{1}{2} + 22\zeta_3 + 28\zeta_3 \ln 2 - \frac{4}{3} - \frac{38\pi^4}{45} + \frac{4\ln^4 2}{3} - \frac{4}{3}\pi^2 \ln^2 2 \right) C_F C_A \right]. \quad (40)$$

5 Numerical check for thrust and heavy jet mass

As a check on our results, we can use the soft function to calculate the soft contribution to the differential thrust and heavy jet mass distributions. The singular parts of these distributions at $\mathcal{O}(\alpha_s^2)$ were previously determined up to four numbers: the coefficients of $\delta(\tau)$ and $\delta(\rho)$ for the $C_F C_A$ and $C_F n_f T_F$ color structures. Until now these four numbers were unknown and had to be fit numerically using the EVENT 2 program. We can now use our results for the hemisphere soft function to replace these numerically fit numbers with analytical results. The coefficients of the δ -functions are the same as the constant terms in $R_\rho(\rho)$ and $R_\tau(\tau)$, for which formulae were given in the previous section.

The unknown soft contributions to the coefficients of $\delta(\tau)$ and $\delta(\rho)$ were denoted c_2^S and $c_{2\rho}^S$ in [12]. We find

$$c_2^S = \frac{\pi^4}{2} C_F^2 + \left(-\frac{2140}{81} - \frac{871\pi^2}{54} + \frac{14\pi^4}{15} + \frac{286\zeta_3}{9} \right) C_F C_A \\ + \left(\frac{80}{81} + \frac{154\pi^2}{27} - \frac{104\zeta_3}{9} \right) C_F n_f T_F, \quad (41)$$

$$c_{2\rho}^S = \frac{\pi^4}{2} C_F^2 + \left(-\frac{2032}{81} - \frac{871\pi^2}{54} + \frac{16\pi^4}{9} - \frac{4\ln^4 2}{3} + \frac{4}{3}\pi^2 \ln^2 2 - 28\zeta_3 \ln 2 \right. \\ \left. + \frac{88\zeta_3}{9} - 32\text{Li}_4\left(\frac{1}{2}\right) \right) C_F C_A + \left(-\frac{136}{81} + \frac{154\pi^2}{27} - \frac{32\zeta_3}{9} \right) C_F n_f T_F. \quad (42)$$

These numbers were fit numerically in [11, 12, 15] based on a method introduced in [11]. The procedure involves subtracting the singular parts of the thrust and heavy jet mass distributions, which are known analytically from SCET, up to delta-function terms, from the full QCD distributions for thrust and heavy jet mass calculated numerically with the program EVENT 2. The difference is then integrated over and compared to the total cross section, which is known analytically, minus the analytic integral over the singular terms. The highest precision fits were done in [12] so we compare only to those. The result is

$$c_2^S = (48.7045)C_F^2 + (-56.4990)C_F C_A + (43.3905)C_F n_f T_F \quad (\text{analytic result}) \\ = (49.1)C_F^2 + (-57.8)C_F C_A + (43.4)C_F n_f T_F \quad (\text{fit result [12]}) \quad (43)$$

and $c_{2\rho}^S$

$$\begin{aligned} c_{2\rho}^S &= (48.7045)C_F^2 + (-33.2286)C_F C_A + (50.3403)C_F n_f T_F && \text{(analytic result)} \\ &= (49.1)C_F^2 + (-33.2)C_F C_A + (50.2)C_F n_f T_F && \text{(fit result [12])}. \end{aligned} \quad (44)$$

The percent errors for these numbers are 0.8%, 2%, 0.02% for c_2^S and 0.8%, 0.08% and 0.2% for $c_{2\rho}^S$ respectively, with an average error of around 0.5%. This is excellent agreement. Note that the C_F^2 terms were already known when the fits were done, so small errors were expected.

For completeness, the complete contributions of the soft function to $\delta(\rho)$ and $\delta(\tau)$, denoted by $D_\delta^{(\rho)}$ and $D_\delta^{(\tau)}$ at order α_s^2 are

$$\begin{aligned} D_\delta^{(\tau)} &= \left(\frac{\alpha_s}{4\pi}\right)^2 \left\{ c_2^S - \frac{4}{5}\pi^4 C_F^2 + C_F C_A \left(\frac{352\zeta_3}{9} + \frac{268\pi^2}{27} - \frac{4\pi^4}{9} \right) + C_F T_F n_f \left(-\frac{128\zeta_3}{9} - \frac{80\pi^2}{27} \right) \right\}, \\ D_\delta^{(\rho)} &= \left(\frac{\alpha_s}{4\pi}\right)^2 \left\{ c_{2\rho}^S - \frac{28}{45}\pi^4 C_F^2 + C_F C_A \left(\frac{352\zeta_3}{9} + \frac{268\pi^2}{27} - \frac{4\pi^4}{9} \right) + C_F T_F n_f \left(-\frac{128\zeta_3}{9} - \frac{80\pi^2}{27} \right) \right\}. \end{aligned} \quad (45)$$

One can also use c_2^S and $c_{2\rho}^S$ to get the complete coefficient of $\delta(\tau)$ and $\delta(\rho)$ including jet and hard function contributions, using Appendices C of Refs. [11] and [12].

6 Hemisphere mass distribution

The numerical check performed in the previous section provides strong evidence that our analytical results are correct. With these results in hand, we can now compare to other features of the hemisphere mass distribution and the integrated hemisphere soft function, $\mathcal{R}(X, Y, \mu)$.

The entire μ -dependence of $\mathcal{R}(X, Y, \mu)$ is predicted by SCET. Indeed, renormalization group invariance predicts that the differential soft function must factorize in Laplace space, as in Eq. (1). The Laplace transform is defined by

$$\tilde{s}(x_L, x_R, \mu) = \int_0^\infty dk_L \int_0^\infty dk_R S(k_L, k_R, \mu) e^{-x_L k_L e^{-\gamma_E}} e^{-x_R k_R e^{-\gamma_E}}, \quad (46)$$

where the γ_E factors are added in the definition to avoid their appearance elsewhere. The factorization theorem then implies

$$\tilde{s}(x_L, x_R, \mu) = \tilde{s}_\mu(\ln x_L \mu) \tilde{s}_\mu(\ln x_R \mu) \tilde{s}_f(x_L, x_R). \quad (47)$$

The RG-kernel $\tilde{s}_\mu(L)$ is determined by the renormalization group invariance of the factorization formula, and is expressible in terms of the anomalous dimensions of the hard and jet functions, which are known up to α_s^3 . The finite part $\tilde{s}_f(L)$, until now, has been known only to α_s . This Laplace form leads to a simple expression for the integrated soft function in SCET [12]

$$\mathcal{R}(X, Y, \mu) = \tilde{s}(\partial_{\eta_1}, \partial_{\eta_2}, \mu) \left(\frac{X}{\mu}\right)^{\eta_1} \frac{e^{-\gamma_E \eta_1}}{\Gamma(\eta_1 + 1)} \left(\frac{Y}{\mu}\right)^{\eta_2} \frac{e^{-\gamma_E \eta_2}}{\Gamma(\eta_2 + 1)} \Big|_{\eta_1=\eta_2=0}. \quad (48)$$

The μ -dependent terms in the order α_s^2 integrated soft function calculated in this way agree exactly with the μ -dependent terms in $\mathcal{R}(X, Y, \mu)$. In fact, it is helpful to separate out those terms. To that end, we write the α_s^2 terms as

$$\mathcal{R}(X, Y, \mu) = \left(\frac{\alpha_s}{4\pi}\right)^2 \left[\mathcal{R}_\mu \left(\frac{X}{\mu}, \frac{Y}{\mu} \right) + \mathcal{R}_f \left(\frac{X}{Y} \right) \right], \quad (49)$$

where $\mathcal{R}_\mu(X/\mu, Y/\mu)$ is the part coming directly from the $\tilde{s}_\mu(L)$ terms and $\mathcal{R}_f(X/Y)$ is the remainder, which comes from $\tilde{s}_f(x_L, x_R)$. The result for $\mathcal{R}_\mu(X/\mu, Y/\mu)$ is

$$\begin{aligned} \mathcal{R}_\mu \left(\frac{X}{\mu}, \frac{Y}{\mu} \right) = & \left[8 \ln^4 \frac{X}{\mu} - \frac{20}{3} \pi^2 \ln^2 \frac{X}{\mu} + 16 \ln^2 \frac{X}{\mu} \ln^2 \frac{Y}{\mu} \right. \\ & \left. + 64 \zeta_3 \ln \frac{XY}{\mu^2} + 8 \ln^4 \frac{Y}{\mu} - \frac{20}{3} \pi^2 \ln^2 \frac{Y}{\mu} - \frac{28\pi^4}{45} \right] C_F^2 \\ & + \left[\frac{88}{9} \ln^3 \frac{X}{\mu} + \frac{4}{3} \pi^2 \ln^2 \frac{X}{\mu} - \frac{268}{9} \ln^2 \frac{X}{\mu} - \frac{22}{9} \pi^2 \ln \frac{XY}{\mu^2} + \frac{808}{27} \ln \frac{XY}{\mu^2} \right. \\ & \left. - 28 \zeta_3 \ln \frac{XY}{\mu^2} + \frac{88}{9} \ln^3 \frac{Y}{\mu} + \frac{4}{3} \pi^2 \ln^2 \frac{Y}{\mu} - \frac{268}{9} \ln^2 \frac{Y}{\mu} + \frac{352 \zeta_3}{9} - \frac{4\pi^4}{9} + \frac{268\pi^2}{27} \right] C_F C_A \\ & + \left[-\frac{32}{9} \ln^3 \frac{X}{\mu} + \frac{80}{9} \ln^2 \frac{X}{\mu} + \frac{8}{9} \pi^2 \ln \frac{XY}{\mu^2} - \frac{224}{27} \ln \frac{XY}{\mu^2} \right. \\ & \left. - \frac{32}{9} \ln^3 \frac{Y}{\mu} + \frac{80}{9} \ln^2 \frac{Y}{\mu} - \frac{128 \zeta_3}{9} - \frac{80\pi^2}{27} \right] C_F T_F n_f. \end{aligned} \quad (50)$$

The part of the soft function not determined by RG-invariance is represented entirely by $\tilde{s}_f(x_L, x_R)$. This function is μ -independent and can only depend on the ratio x_L/x_R by dimensional analysis. Moreover, it is symmetric in $x_L \leftrightarrow x_R$, since the hemisphere soft function is symmetric in $k_L \leftrightarrow k_R$. Hoang and Kluth claimed [15] that it should only have logarithms, and up to order α_s^2 , only have \ln^0 and \ln^2 terms. Their ansatz was that

$$\tilde{s}_f(x_L, x_R)^{\text{Hoang-Kluth}} = 1 + \left(\frac{\alpha_s}{4\pi}\right) c_1^S + \left(\frac{\alpha_s}{4\pi}\right)^2 [c_2^S + c_{2L}^S \ln^2 \frac{x_L}{x_R}], \quad (51)$$

with $c_1^S = -C_F \pi^2$ already known.

To check the Hoang-Kluth ansatz, the easiest approach is to look at the contribution of $\tilde{s}_f(x_L, x_R)$ to $\mathcal{R}(X, Y, \mu)$, which we called $\mathcal{R}_f(X/Y)$. For the Hoang-Kluth ansatz, the result is

$$\mathcal{R}_f(z)^{\text{Hoang-Kluth}} = c_2^S + c_{2L}^S (\ln^2 z - \frac{\pi^2}{3}). \quad (52)$$

The values of c_2^S and c_{2L}^S which get right the singular parts of the thrust and heavy jet mass distributions are given in Eqs. (41) and (42) with $c_{2L}^S = \frac{3}{\pi^2} (c_2^S - c_{2\rho}^S)$.

The exact answer, at order α_s^2 is

$$\begin{aligned}
\mathcal{R}_f(z) = & \frac{\pi^4}{2} C_F^2 + \left[-44\text{Li}_3\left(-\frac{1}{z}\right) - 44\text{Li}_3(-z) - 16\text{Li}_4\left(\frac{1}{z+1}\right) - 16\text{Li}_4\left(\frac{z}{z+1}\right) \right. \\
& + \frac{88}{3}\text{Li}_2(-z) \ln z - 4\text{Li}_3\left(-\frac{1}{z}\right) \ln z - 4\text{Li}_3(-z) \ln z + 8\text{Li}_3\left(-\frac{1}{z}\right) \ln(z+1) \\
& + 8\text{Li}_3(-z) \ln(z+1) + 8\zeta_3 \ln z - 16\zeta_3 \ln(z+1) + \frac{2\ln^4 z}{3} \\
& - \frac{4}{3}\ln^4(z+1) - \frac{4}{3}\ln(z+1)\ln^3 z + \frac{22\ln^3 z}{3} + \frac{8}{3}\ln^3(z+1)\ln z \\
& - \frac{2}{3}\pi^2 \ln^2 z + \frac{4}{3}\pi^2 \ln^2(z+1) - \frac{4}{3}\pi^2 \ln(z+1)\ln z + \frac{22\pi^2 z \ln z}{9(z+1)} \\
& - \frac{4z \ln z}{3(z+1)} + \frac{22\pi^2 \ln z}{9(z+1)} + \frac{4 \ln z}{3(z+1)} - \frac{154\zeta_3}{3} + \frac{16\pi^4}{9} - \frac{871\pi^2}{54} - \frac{2032}{81} \\
& \left. + \frac{22\psi^{(2)}(1)}{9} \right] C_F C_A + \left[\frac{2}{81} (1296\text{Li}_3(-z) - 432\text{Li}_2(-z) \ln z + 828\zeta_3 \right. \\
& \left. + (231\pi^2 - 68) + 36 \left(\frac{3(z-1)}{z+1} + 2\pi^2 \right) \ln z \right] C_F n_f T_F
\end{aligned} \tag{53}$$

This is clearly very different from the Hoang-Kluth form.

7 Asymptotic behavior and non-global logs

The factorization theorem is valid in the dijet limit when the hemisphere masses are small compared to Q ; however, there is no restriction on the relative size of the two masses. In addition to logarithms $\ln \frac{M_{L,R}}{\mu}$ required by RG invariance, there may be logarithms of the form $\ln \frac{M_L}{M_R}$ that enter at order α_s^2 . These logarithms cannot be predicted by RG invariance and are known as non-global logarithms. Salam and Dasgupta have shown that non-global logs appear in distributions such as the light jet mass. They argued that in the soft limit, when $M_L \ll M_R$, the leading non-global log should be $-(\frac{\alpha_s}{4\pi})^2 \frac{4\pi^2}{3} C_F C_A \ln^2 \frac{M_L^2}{M_R^2}$ in full QCD.

Non-global logs must be present in SCET, since for small M_L and M_R , the entire distribution is determined by soft and collinear degrees of freedom. However, SCET may not be able to resum these logs. The non-global logs cannot come from the hard function, which has no knowledge of either mass, or the jet function, since each jet function knows about only one mass. Thus they must come from the soft function. Moreover since, by definition, they are not determined by RG invariance, they must be present in the μ -independent part, $\mathcal{R}_f(X/Y)$ of the integrated hemisphere soft function, $\mathcal{R}(X, Y, \mu)$. This function was given explicitly in Eq. (53).

To see the non-global logs in $\mathcal{R}_f(z)$ we can simply take the limit $z \rightarrow \infty$. Note that $\mathcal{R}_f(z) = \mathcal{R}_f(\frac{1}{z})$ so this is also the limit $z \rightarrow 0$. The asymptotic limit of $\mathcal{R}_f(z)$ for large or

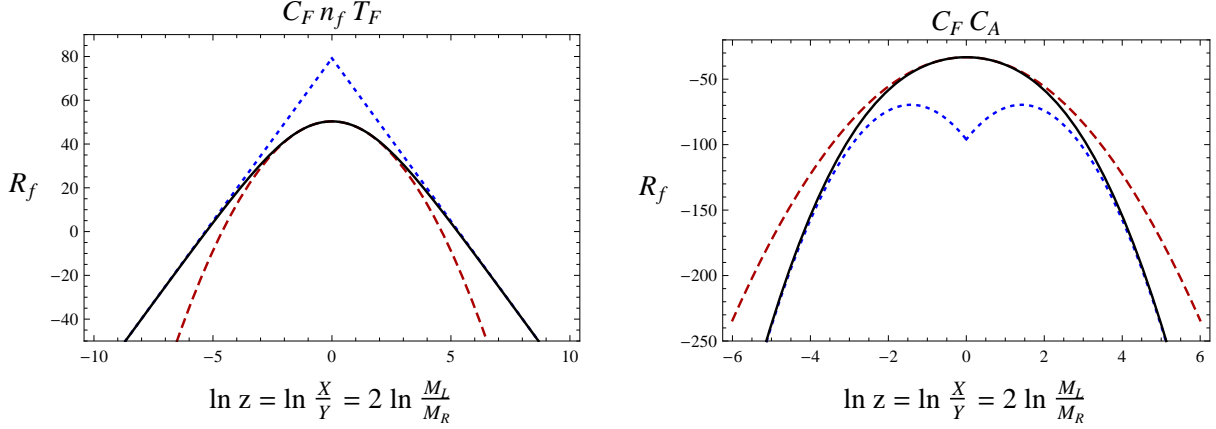


Figure 6: The contribution of the part of the soft function not fixed by renormalization group invariance to the hemisphere mass distribution, $\mathcal{R}_f(z)$ is shown. On the left is the $C_F n_f T_F$ color factor and on the right is $C_F C_A$, both as a function of $\ln z \equiv \ln \frac{X}{Y}$. The solid black curve is the exact result of Eq. (53). The dashed red curve is the plot of the small $\ln z$ expression of Eq. (55) and the dotted blue curve give the large $\ln z$ behavior of Eq. (54). The kink is due to a sign flip, since the linear term appears as $|\ln z|$.

small z is

$$\begin{aligned} \mathcal{R}_f^{z \gg 1}(z) &= \frac{\pi^4}{2} C_F^2 + \left[\left(\frac{8}{3} - \frac{16\pi^2}{9} \right) |\ln z| + \frac{136}{81} + \frac{154\pi^2}{27} + \frac{184\zeta_3}{9} \right] C_F n_f T_F \\ &+ \left[-\frac{4}{3} \pi^2 \ln^2 z + \left(-8\zeta_3 - \frac{4}{3} + \frac{44\pi^2}{9} \right) |\ln z| - \frac{506\zeta_3}{9} + \frac{8\pi^4}{5} - \frac{871\pi^2}{54} - \frac{2032}{81} \right] C_F C_A. \end{aligned} \quad (54)$$

There are two important features to note in this expansion. First of all, in the $C_F C_A$ color structure there is a term $-\frac{4\pi^2}{3} \ln^2 z$, which is the leading non-global log found by Dasgupta and Salam. But we also see that there are sub-leading non-global logs, of the form $|\ln z|$. The absolute value is necessary to keep the expression symmetric in $z \rightarrow \frac{1}{z}$. It is interesting to see how this sign flip comes out of the full analytic expression.

Next, let us look at $z \sim 1$. Here we find

$$\begin{aligned} \mathcal{R}_f^{z \sim 1}(z) &= \frac{\pi^4}{2} C_F^2 + \left[\left(-\frac{2}{3} - \frac{4\pi^2}{3} - 4 \ln^2 2 + \frac{44 \ln 2}{3} \right) \ln^2 z - 32 \text{Li}_4 \left(\frac{1}{2} \right) + \frac{88\zeta_3}{9} \right. \\ &\quad \left. - 28\zeta_3 \ln(2) - \frac{2032}{81} - \frac{871\pi^2}{54} + \frac{16\pi^4}{9} - \frac{4 \ln^4 2}{3} + \frac{4}{3} \pi^2 \ln^2 2 \right] C_F C_A \\ &+ \left[\left(\frac{4}{3} - \frac{16 \ln 2}{3} \right) \ln^2 z + \frac{154\pi^2}{27} - \frac{136}{81} - \frac{32\zeta_3}{9} \right] C_F n_f T_F + \mathcal{O}(\ln^3 z). \end{aligned} \quad (55)$$

We see there is a double logarithmic term for both the $C_F C_A$ and $C_F n_f T_F$ color structures. This is consistent with an analysis performed in [15] of an observable $\rho^\alpha = \max(\alpha M_L^2, M_R^2)/Q^2$.

They found that the integrated ρ^α distribution looked like $\ln^2 \alpha$ for $\alpha \sim 1$. This quadratic behavior in $\ln \alpha$ corresponds exactly to the quadratic behavior in the $z \sim 1$ limit in (55).

We show in Figure 6 the exact finite function $\mathcal{R}_f(z)$ and a comparison to its asymptotic behavior at small $\ln z$ and large $\ln z$ for the $C_F C_A$ and $C_F n_f T_F$ color structures. For both color structures, the exact curve is well approximated by a parabola for small $\ln z$. At large $\ln z$, for the $C_F n_f T_F$ color factor, the exact result approaches a linear function whereas the $C_F C_A$ color structure has $\ln^2 z$ dependence with a different coefficient than for the small $\ln z$ limit. The $C_F C_A$ term has a linear term as well.

As we have discussed, the integrated hemisphere soft function contributes directly to the doubly differential hemisphere mass distribution. In the limit where both hemisphere masses are small, and well separated, the soft function gives the dominant contribution. In this regime, we can read off that the leading non-global logarithms are given by $\mathcal{R}_f^{z \gg 1}(M_L^2/M_R^2)$ in Eq.(54). The \ln^2 term has an identical coefficient to that found in [26]. The subleading non-global logarithm is a new result.

These non-global logarithms become important when one scale becomes parametrically larger than the other. The separation of scales suggest that at the higher of the two scales, one may be able to match onto a new effective theory and then run the matching coefficient between the two scales. In fact, the $-\frac{4\pi^2}{3} \ln^2 z$ term in this calculation has its origin in $f(0,0)$, where $f(r, \epsilon)$ is the opposite-direction contribution to the hemisphere soft function, as in the Appendix. Indeed, we found that

$$f_{C_A}(0, \epsilon) = \frac{8\pi^2}{3} + \mathcal{O}(\epsilon), \quad f_{n_f}(0, \epsilon) = \mathcal{O}(\epsilon^2), \quad (56)$$

which is consistent with the leading non-global logarithm only having the $C_F C_A$ color structure. Since it is the ϵ^0 part of this expression which contributes, and there are double soft poles, the full expansion also has terms like $f(0,0) \ln^2 \mu$. Thus $f(0,0)$ can be thought of as an anomalous dimension, providing hope that these non-global logs might be resummed in an effective theory. A consistent framework may require some kind of refactorization, like the one found a related event shape, τ_ω , in [25]. However, it is not clear whether a complete consistent matching and running scheme can be set up for non-global logs, so we leave such considerations to future work.

8 Conclusions

In this paper, we have presented the complete calculation of the hemisphere soft function to order α_s^2 . This is the first 2-loop calculation of a soft function which depends on two scales in addition to the renormalization group scale μ . The hemisphere soft function, $S(k_L, k_R, \mu)$, depends on the components of the momenta going into the left and right hemispheres. In a one-scale soft function, such as the Drell-Yan soft function, $S_{DY}(k, \mu)$ [22, 23, 30], the thrust soft function $S_T(k, \mu)$ [9, 11] or the direct photon soft function $S_\gamma(k, \mu)$ [16], all of the k dependence is fixed once the μ -dependence is known. Since the μ -dependence is fixed by RG invariance, these functions are often completely determined. For multi-scale soft functions, like the hemisphere soft function, there can be additional dependence on the ratio $r = k_L/k_R$.

We worked out this dependence explicitly at order α_s^2 , and the result is more complicated than previously anticipated.

We performed a number of checks on our calculation. The μ -dependence of the result was entirely known by the factorization theorem in SCET, and we have confirmed that the μ -dependence of our hemisphere soft function matches the result obtained from factorization analysis. In addition, the result allows us to produce analytic expressions for all of the singular terms in the 2-loop thrust and heavy jet mass distributions. The constant terms in the singular distributions were previously unknown and had to be extracted from numerical fits [11, 15, 12]. We found our analytical results to be in excellent agreement with the very precise recent numerical fit of [12].

The full hemisphere soft function produces the leading and sub-leading non-global logs in the hemisphere mass distribution. Previously, only the leading double-log term was known, from a calculation in the soft limit of full QCD [26]. In this work we reproduced that double logarithm and, furthermore, showed the existence of a sub-leading single logarithm. This single logarithm, of M_L/M_R , is interesting because $\ln M_L/M_R$ seems like it should be forbidden by the $M_L \leftrightarrow M_R$ symmetry. Curiously, we find that the complicated behavior of the hemisphere mass distribution when $M_L \sim M_R$ allows the single log to flip sign and it manifests itself as $\ln[\max(M_L, M_R)/\min(M_L, M_R)] = |\ln M_L/M_R|$. Our calculation is the first to exhibit a sub-leading non-global logarithm of this type.

Besides being of formal interest, the hemisphere soft function at $\mathcal{O}(\alpha_s^2)$ is a crucial component of the resummed heavy-jet mass distribution at N³LL order. Previous fits to α_s at this order assumed a simple form for the soft function, using the Hoang-Kluth ansatz. We have shown that this ansatz is valid only in the limit that $k_L \sim k_R$. With the exact $\mathcal{O}(\alpha_s^2)$ soft function in hand, one source of uncertainty in the α_s fits to event shapes can be removed.

This work also has implications for calculations of distributions at hadron colliders. At hadron colliders, there are necessarily many more scales in relevant observables than at e^+e^- machines. For example, jet sizes and veto scales play a critical role in many analysis [31, 21, 25]. For multi-scale observables to be computed in effective field theory, we need a better understanding of multi-scale soft functions, such as this exact result on the 2-loop hemisphere soft function provides.

9 Acknowledgements

The authors would like to thank C. Lee, K. Melnikov and I. Stewart for useful discussions and F. Petriello and I. Scimemi for collaboration on intermediate stages of this project. RK and MDS were supported in part by the Department of Energy, under grant DE-SC003916. HXZ was supported by the National Natural Science Foundation of China under grants No. 11021092 and No. 10975004 and the Graduate Student academic exchange program of Peking University.

A Opposite direction contributions

The following are the first 3 terms in the ϵ expansion of f_{C_A} from Eq. (17).

$$f_{C_A}^{(0)}(r) = 8 \left(\frac{r(11r^2 + 21r + 12) \ln(r)}{3(r+1)^3} + \frac{\pi^2(r+1)^2 + 2r}{3(r+1)^2} + \ln^2(r+1) - \ln(r) \ln(r+1) - \frac{11}{3} \ln(r+1) \right), \quad (57)$$

$$\begin{aligned} f_{C_A}^{(1)}(r) = & 8 \left(\frac{(-11r^3 - 9r^2 + 9r + 11) \text{Li}_2(-r)}{3(r+1)^3} + 3\text{Li}_3(-r) - 2\text{Li}_2(-r) \ln(r) \right. \\ & + \frac{r(11r^2 + 21r + 12) \ln^2(r)}{6(r+1)^3} - \frac{10r(7r^2 + 15r + 6) \ln(r)}{9(r+1)^3} \\ & + \frac{r^3(36\zeta_3 - 11\pi^2) + r^2(108\zeta_3 - 20 - 21\pi^2) - 4r(-27\zeta_3 + 5 + 3\pi^2) + 36\zeta_3}{18(r+1)^3} \\ & + \frac{(-11r^3 - 9r^2 + 9r + 11) \ln(r+1) \ln(r)}{3(r+1)^3} - \frac{1}{2} \ln(r+1) \ln^2(r) \\ & \left. + \frac{1}{18} (140 + 3\pi^2) \ln(r+1) \right) \\ & + 256\pi^4 \left(-\frac{r^2(r+3) \ln(r) + 2r(r+1) + (r+1)^3 \ln(r+1)}{96\pi^4(r+1)^3} \right), \quad (58) \end{aligned}$$

$$\begin{aligned} f_{C_A}^{(2)}(r) = & \text{Li}_2(-r) \left(\frac{8(-r^3 - 3r^2 + 3r + 1)}{3(r+1)^3} + \frac{80(7r^3 + 9r^2 - 9r - 7)}{9(r+1)^3} + \frac{8(33r^3 + 75r^2 + 57r + 11) \ln(r)}{3(r+1)^3} \right. \\ & \left. + \frac{16(-11r^3 - 9r^2 + 9r + 11) \ln(r+1)}{3(r+1)^3} - 8 \ln^2(r) + 16 \ln(r+1) \ln(r) \right) \\ & + \text{Li}_3(-r) \left(\frac{8(-55r^3 - 117r^2 - 81r - 11)}{3(r+1)^3} + 8 \ln(r) \right) \\ & + \text{Li}_3 \left(\frac{1}{r+1} \right) \left(\frac{32(-11r^3 - 9r^2 + 9r + 11)}{3(r+1)^3} + 16 \ln(r) \right) - 16\text{Li}_4 \left(\frac{1}{r+1} \right) \\ & - 16\text{Li}_4 \left(\frac{r}{r+1} \right) + \zeta_3 \left(-\frac{128r^2}{(r+1)^3} - \frac{224r}{(r+1)^3} - \frac{352}{3(r+1)^3} - 16 \ln(r) + 16 \ln(r+1) \right) \\ & + \frac{8\pi^2 r(35r^2 + 78r + 33)}{27(r+1)^3} - \frac{4r(\pi^2 r^2 + (3\pi^2 - 20)r - 20)}{9(r+1)^3} + \frac{16r^2}{27(r+1)^3} \\ & - \frac{32(12r^2 + 21r + 11) \ln^3(r+1)}{9(r+1)^3} + \frac{4r(11r^2 + 21r + 12) \ln^3(r)}{9(r+1)^3} \end{aligned}$$

$$\begin{aligned}
& + \frac{16(12r^2 + 21r + 11)\ln(r)\ln^2(r+1)}{3(r+1)^3} + \frac{4r^2(r+3)\ln^2(r)}{3(r+1)^3} - \frac{40r(7r^2 + 15r + 6)\ln^2(r)}{9(r+1)^3} \\
& - \frac{16r(r^2 - 3r + 6)\ln(r)}{9(r+1)^3} + \frac{16r(196r^2 + 375r + 195)\ln(r)}{27(r+1)^3} \\
& + \frac{4(-11r^3 - 9r^2 + 9r + 11)\ln^2(r)\ln(r+1)}{3(r+1)^3} \\
& - \frac{8(\pi^2(66r^3 + 90r^2 + 9r - 33) + 4(98r^3 + 285r^2 + 285r + 98))\ln(r+1)}{27(r+1)^3} \\
& - \frac{8(r^3 + 3r^2 - 3r - 1)\ln(r)\ln(r+1)}{3(r+1)^3} \\
& + \frac{8(70r^3 + 78r^2 - 102r + 3\pi^2(r+1)^3 - 70)\ln(r)\ln(r+1)}{9(r+1)^3} + \frac{16r}{27(r+1)^3} \\
& - \frac{4}{3}\ln^4(r+1) - \frac{4}{3}\ln^3(r)\ln(r+1) + 8\ln^2(r)\ln^2(r+1) \\
& + \frac{32r\ln^2(r+1)}{3(r+1)^2} + \frac{16}{9}\ln(r+1) + \frac{44\pi^4}{45}. \tag{59}
\end{aligned}$$

The following are the first 2 terms in the ϵ expansion of f_{n_f} from Eq. (28).

$$f_{n_f}^{(0)}(r) = -\frac{16(2r(r+1) - 2(r+1)^3\ln(r+1) + r(r(2r+3) + 3)\ln(r))}{3(r+1)^3}, \tag{60}$$

$$\begin{aligned}
f_{n_f}^{(1)}(r) = & \frac{8}{9(r+1)^3} \left(-12(r^3 - 1)\text{Li}_2\left(-\frac{1}{r}\right) - 32r^3\ln(r+1) + 3\pi^2r^2 + 20r^2 \right. \\
& - 96r^2\ln(r+1) - 3(4r^3 + 3r^2 + 3r - 2)\ln^2(r) + 4\ln(r)(3(r^3 - 1)\ln(r+1) \\
& \left. + r(8r^2 + 21r + 3)) + 3\pi^2r + 20r - 96r\ln(r+1) - 32\ln(r+1) + 2\pi^2 \right). \tag{61}
\end{aligned}$$

References

- [1] A. Gehrmann-De Ridder, T. Gehrmann and E. W. N. Glover, JHEP **0509**, 056 (2005) [arXiv:hep-ph/0505111].
- [2] A. Gehrmann-De Ridder, T. Gehrmann, E. W. N. Glover and G. Heinrich, Phys. Rev. Lett. **99**, 132002 (2007) [arXiv:0707.1285 [hep-ph]].
- [3] A. Gehrmann-De Ridder, T. Gehrmann, E. W. N. Glover and G. Heinrich, JHEP **0712**, 094 (2007) [arXiv:0711.4711 [hep-ph]].
- [4] S. Weinzierl, Phys. Rev. Lett. **101**, 162001 (2008) [arXiv:0807.3241 [hep-ph]].
- [5] C. W. Bauer, S. Fleming, D. Pirjol and I. W. Stewart, Phys. Rev. D **63**, 114020 (2001) [arXiv:hep-ph/0011336].
- [6] C. W. Bauer, D. Pirjol and I. W. Stewart, Phys. Rev. D **65**, 054022 (2002) [arXiv:hep-ph/0109045].
- [7] M. Beneke, A. P. Chapovsky, M. Diehl and T. Feldmann, Nucl. Phys. B **643**, 431 (2002) [arXiv:hep-ph/0206152].
- [8] S. Fleming, A. H. Hoang, S. Mantry and I. W. Stewart, Phys. Rev. D **77**, 074010 (2008) [arXiv:hep-ph/0703207].
- [9] M. D. Schwartz, Phys. Rev. D **77**, 014026 (2008) [arXiv:0709.2709 [hep-ph]].
- [10] T. Becher and M. Neubert, Phys. Lett. B **637**, 251 (2006) [arXiv:hep-ph/0603140].
- [11] T. Becher and M. D. Schwartz, JHEP **0807**, 034 (2008) [arXiv:0803.0342 [hep-ph]].
- [12] Y. T. Chien and M. D. Schwartz, JHEP **1008**, 058 (2010) [arXiv:1005.1644 [hep-ph]].
- [13] R. Abbate, M. Fickinger, A. Hoang, V. Mateu and I. W. Stewart, PoS **RADCOR2009**, 040 (2010) [arXiv:1004.4894 [hep-ph]].
- [14] W. M. Yao *et al.* [Particle Data Group], J. Phys. G **33**, 1 (2006).
- [15] A. H. Hoang and S. Kluth, arXiv:0806.3852 [hep-ph].
- [16] T. Becher and M. D. Schwartz, JHEP **1002**, 040 (2010) [arXiv:0911.0681 [hep-ph]].
- [17] N. Kidonakis, G. F. Sterman, Nucl. Phys. **B505**, 321-348 (1997). [hep-ph/9705234].
- [18] S. M. Aybat, L. J. Dixon, G. F. Sterman, Phys. Rev. **D74**, 074004 (2006). [hep-ph/0607309].
- [19] R. Kelley, M. D. Schwartz, Phys. Rev. **D83**, 033001 (2011). [arXiv:1008.4355 [hep-ph]].
- [20] R. Kelley, M. D. Schwartz, Phys. Rev. **D83**, 045022 (2011). [arXiv:1008.2759 [hep-ph]]. ,1002,040;

- [21] S. D. Ellis, C. K. Vermilion, J. R. Walsh, A. Hornig and C. Lee, arXiv:1001.0014 [hep-ph].
- [22] G. P. Korchemsky and G. Marchesini, Phys. Lett. B **313**, 433 (1993).
- [23] A. V. Belitsky, Phys. Lett. B **442**, 307 (1998) [arXiv:hep-ph/9808389].
- [24] T. Becher and M. Neubert, Phys. Lett. B **633**, 739 (2006) [arXiv:hep-ph/0512208].
- [25] R. Kelley, M. D. Schwartz and H. X. Zhu, arXiv:1102.0561 [hep-ph].
- [26] M. Dasgupta and G. P. Salam, Phys. Lett. B **512**, 323 (2001) [arXiv:hep-ph/0104277].
- [27] S. Fleming, A. H. Hoang, S. Mantry and I. W. Stewart, Phys. Rev. D **77**, 114003 (2008) [arXiv:0711.2079 [hep-ph]].
- [28] T. Huber and D. Maitre, Comput. Phys. Commun. **175**, 122 (2006) [arXiv:hep-ph/0507094].
- [29] G. Heinrich, Int. J. Mod. Phys. A **23**, 1457 (2008) [arXiv:0803.4177 [hep-ph]].
- [30] T. Becher, M. Neubert and G. Xu, JHEP **0807**, 030 (2008) [arXiv:0710.0680 [hep-ph]].
- [31] S. D. Ellis, A. Hornig, C. Lee, C. K. Vermilion, J. R. Walsh, Phys. Lett. **B689**, 82-89 (2010). [arXiv:0912.0262 [hep-ph]].